Noninvasive assessment of the rheological behavior of human organs using multifrequency MR elastography: a study of brain and liver viscoelasticity

To cite this article: Dieter Klatt *et al* 2007 *Phys. Med. Biol.* **52** 7281

IOP Publishing Physics in Medicine and Biology

Phys. Med. Biol. **52** (2007) 7281–7294 doi:10.1088/0031-9155/52/24/006

Noninvasive assessment of the rheological behavior of human organs using multifrequency MR elastography: a study of brain and liver viscoelasticity

Dieter Klatt[1], **Uwe Hamhaber**[2], **Patrick Asbach**[1], **Jürgen Braun**[2] **and Ingolf Sack**[1]

[1] Department of Radiology, Charité–Universitätsmedizin Berlin, Campus Charité Mitte, Charitéplatz 1, 10117 Berlin, Germany
[2] Institute of Medical Informatics, Charité–Universitätsmedizin Berlin, Campus Benjamin Franklin, Hindenburgdamm 30, 12200 Berlin, Germany

E-mail: ingolf.sack@charite.de

Received 8 June 2007, in final form 19 September 2007
Published 23 November 2007
Online at stacks.iop.org/PMB/52/7281

Abstract

MR elastography (MRE) enables the noninvasive determination of the viscoelastic behavior of human internal organs based on their response to oscillatory shear stress. An experiment was developed that combines multifrequency shear wave actuation with broad-band motion sensitization to extend the dynamic range of a single MRE examination. With this strategy, multiple wave images corresponding to different driving frequencies are simultaneously received and can be analyzed by evaluating the dispersion of the complex modulus over frequency. The technique was applied on the brain and liver of five healthy volunteers. Its repeatability was tested by four follow-up studies in each volunteer. Five standard rheological models (Maxwell, Voigt, Zener, Jeffreys and fractional Zener model) were assessed for their ability to reproduce the observed dispersion curves. The three-parameter Zener model was found to yield the most consistent results with two shear moduli $\mu_1 = 0.84 \pm 0.22$ (1.36 ± 0.31) kPa, $\mu_2 = 2.03 \pm 0.19$ (1.86 ± 0.34) kPa and one shear viscosity of $\eta = 6.7 \pm 1.3$ (5.5 ± 1.6) Pa s (interindividual mean $\pm$ SD) in brain (liver) experiments. Significant differences between the rheological parameters of brain and liver were found for μ_1 and η ($P < 0.05$), indicating that human brain is softer and possesses a higher viscosity than liver.

(Some figures in this article are in colour only in the electronic version)

Introduction

Palpation is a standard clinical practice for assessing tissue's health near the surface of the body. This method relies on the stress–strain response of soft biological tissue subjected

to an external force (Fung 1993). In viscoelastic theory, this response can be modeled by a combination of elastic and viscous elements which allow for characterizing the specific rheological (i.e. viscoelastic deformation) behavior of the material (Joseph 1990).

Rheological parameters of living tissue have thus so far been rarely used in medical diagnosis. This is mainly due to the invasive character of most rheological tests based on indentation experiments, rheometers, torsional resonators and oscillatory shear testing devices (Valtorta and Mazza 2006, Liu and Bilston 2000, Nicolle *et al* 2005). In contrast, noninvasive elastography experiments have been developed during the last decade that are capable of 'touching' remote tissue by shear waves and measuring the deflection response of the tissue by ultrasound (Parker *et al* 1998) or MRI (Muthupillai *et al* 1995). *In vivo* elastography has been successfully applied to reveal the stiffness of a variety of human tissues and organs such as muscle (Uffmann *et al* 2004, Gennisson *et al* 2005, Papazoglou *et al* 2006, Bensamoun *et al* 2006), breast (Van Houten *et al* 2003, Bercoff *et al* 2003, Sinkus *et al* 2005), brain (McCracken *et al* 2005, Hamhaber *et al* 2007, Sack *et al* 2007) and liver (Ziol *et al* 2005, Corpechot *et al* 2006, Rouviere *et al* 2006, Huwart *et al* 2006, Klatt *et al* 2006). Apart from pure elasticity measurements, only a few studies have been performed to estimate both elasticity and viscosity of *in vivo* tissue and derive a viscoelastic model that predicts the dynamic strain response seen in elastography (Sinkus *et al* 2005, Sack *et al* 2007).

Viscoelastic parameters can be measured by elastography applying various vibration frequencies, which allows deducing the dispersion (i.e. the frequency dependence) of the wave propagation speed and the wave-damping coefficient (Sack *et al* 2007, Kruse *et al* 2000). Variable driving frequencies must thus be repeatedly applied by conventional elastography experiments. Here, an experiment is introduced that exploits the broad-band nature of frequency encoding in MR elastography (MRE) (Rump *et al* 2007) in order to simultaneously encode multiple shear wave oscillations in a single experiment. The experiment enables measuring the dispersion of wave speeds and wave-damping coefficients at four driving frequencies without any additional exam time. The frequency resolution of MRE data gained is used to evaluate five rheological models frequently used in the literature, which yield two (Voigt model, Maxwell model), three (Zener model, Jeffreys model) or four (fractional Zener model) independent constitutive parameters (Joseph 1990, Schiessel *et al* 1995).

The technique is applied to *in vivo* human brain and liver. Both organs are challenging targets for *in vivo* rheology due to their high shielding by bones combined with their soft and viscous mechanical behavior causing a fast obliteration of shear waves. These experimental challenges are opposed to the enormous interest in accurately measuring rheological parameters of brain and liver. For instance, the biomechanical properties of the brain have been the subject of many recent studies related to hydrocephalus (Taylor and Miller 2004), traumatic brain injury (Bayly *et al* 2006) and the evaluation of stroke or intraoperative evaluation (Kuroiwa *et al* 2006, Scholz *et al* 2005). All these studies are based on invasive experiments. Moreover, the diagnosis of chronic liver diseases is still based on invasive biopsy despite recent advances in determining the degree of liver fibrosis made by elastography (Ziol *et al* 2005, Huwart *et al* 2006). The possibility of using elastography-derived viscoelastic parameters for the diagnosis of hepatic or neurological diseases will depend on their reproducibility under similar experimental conditions. Here, the variability of multifrequent MRE data is assessed by four follow-up studies in five healthy volunteers.

Theory

The basic equations necessary for understanding the data evaluation used in this paper are briefly summarized in the following. Two-dimensional wave images are acquired with through-

plane motion sensitization, henceforth referred to as a scalar wave field $u(x, y, t)$ whose temporal Fourier-transformed is denoted as $U(x, y, \omega)$. Assuming isotropy and pure shear stress, the equation of motion for shear waves in the frequency domain reads

$$\rho\omega^2 U + G(\omega)\Delta U = 0, \qquad \Delta = \left(\frac{\partial^2}{\partial x^2} + \frac{\partial^2}{\partial y^2}\right). \tag{1}$$

$\omega = 2\pi f$ is the angular driving frequency, while $G(\omega)$ and ρ represent the complex shear modulus and the density of the material respectively. Solving equation (1) for G yields

$$G(\omega) = -\frac{\rho\omega^2 U}{\Delta U}. \tag{2}$$

A harmonic plane wave approach is used to attribute G to the shear wave speed c and the wave-damping coefficient γ:

$$u = u_0 \exp\left[\mathrm{i}\omega\left(\frac{\mathbf{n}\cdot\mathbf{r}}{c} - t\right) - \gamma\,\mathbf{n}\cdot\mathbf{r}\right]. \tag{3}$$

$\mathbf{n}$ is the wave normal vector, $\mathbf{r}$ is the position vector and u_0 denotes the initial deflection. Solving equation (2) with equation (3) yields the dispersion relations of wave speed and wave damping:

$$c(\omega) = \frac{1}{\mathrm{Re}\left[\sqrt{\frac{\rho}{G(\omega)}}\right]} \qquad \text{and} \qquad \gamma(\omega) = \omega\,\mathrm{Im}\left[\sqrt{\frac{\rho}{G(\omega)}}\right] \tag{4}$$

with Re and Im as symbols for the real and the imaginary parts of a complex number. The complex modulus can be related to elasticity and viscosity using various rheological models. In this study, the following models $G_M(\omega)$ are used:

$$G_M(\omega) = \begin{cases} \mu + \mathrm{i}\omega\eta & \text{Voigt} \\ \dfrac{\mathrm{i}\omega\eta\mu}{\mu + \mathrm{i}\omega\eta} & \text{Maxwell} \\ \dfrac{\mu_1\mu_2 + \mathrm{i}\omega\eta(\mu_1 + \mu_2)}{\mu_2 + \mathrm{i}\omega\eta} & \text{Zener} \\ -\omega\eta_1\dfrac{\omega\eta_2 - \mathrm{i}\mu}{\mu + \mathrm{i}\omega(\eta_1 + \eta_2)} & \text{Jeffreys} \\ \mu_1 + \dfrac{\mu_2\left(\frac{\mathrm{i}\omega\eta}{\mu_2}\right)^\alpha}{1 + \left(\frac{\mathrm{i}\omega\eta}{\mu_2}\right)^\alpha} & \text{fractional Zener.} \end{cases} \tag{5}$$

Their representations by series-parallel models are shown in figure 1. The number of free viscoelastic parameters increases with the complexity of the model. While the Voigt and Maxwell models require only one shear modulus (μ) and one shear viscosity (η), the Zener model and the Jeffreys model incorporate either an extra shear modulus or a viscosity parameter (Fung 1993, Joseph 1990). The other fractional Zener model (Schiessel *et al* 1995) considered is an extension of the Zener model exchanging the dashpot with a spring pot (see figure 1). This rheological element represents an interpolation between purely elastic and purely viscous behaviors with the weighting factor α ($0 \leqslant \alpha \leqslant 1$). The spring pot can be precisely reduced to a spring and to a dashpot for $\alpha = 0$ and $\alpha = 1$, respectively.

The model-dependent viscoelastic parameters were determined by minimizing the error

$$\chi = \frac{1}{N}\sum_{n=1}^{N}\sqrt{(\mathrm{Re}[G(\omega_n) - G_M(\omega_n)])^2 + (\mathrm{Im}[G(\omega_n) - G_M(\omega_n)])^2}, \tag{6}$$

where N denotes the number of experimental driving frequencies.

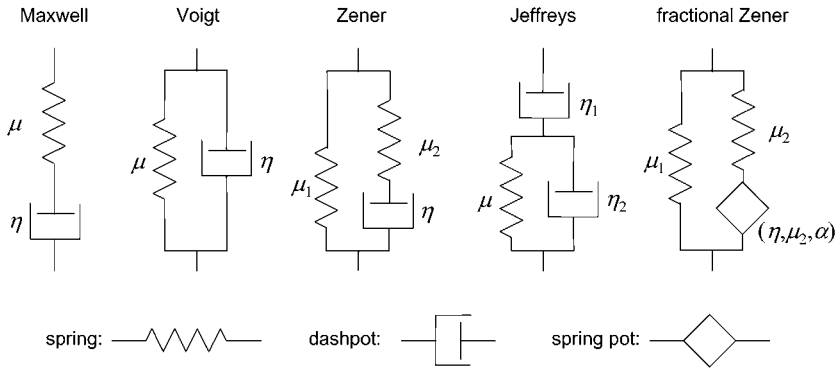

Figure 1. Rheological models used in this study.

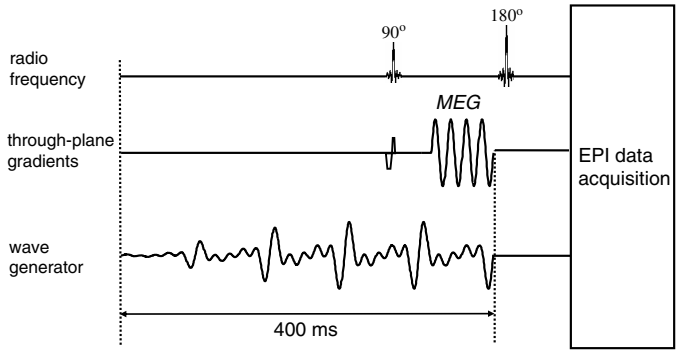

Figure 2. Scheme of the MRE sequence used. The shown motion-encoding gradient (MEG) corresponds to the brain-study setup with four sinusoidal cycles of 60 Hz frequency.

Methods

Multifrequent MRE experiments were applied to the brain and liver of five healthy male volunteers aged 25, 34, 35, 37 and 46 years. Each subject and organ was examined four times with the same protocol over a period of 3 months. Institutional review board approval was obtained, and informed consent was obtained for all subjects.

Wave image acquisition

Experiments were run on a 1.5 T scanner (Magnetom Sonata; Siemens Medical Solutions, Erlangen, Germany). A single-shot SE (spin-echo) EPI (echo planar imaging) sequence with a sinusoidal motion-encoding gradient (MEG) in the through-plane direction and of frequency f_g was used to acquire transverse phase contrast wave images (figure 2). At the beginning of the sequence, a TTL-trigger pulse was given to the wave generator. The trigger delay was increased 40 times by an increment of 2 ms to achieve a frequency resolution of 12.5 Hz multiples. At each time point, two phase images with inverse MEG amplitude were acquired to calculate phase-difference wave images. Further acquisition parameters in brain (liver): $f_g = 60$ (50) Hz, number of MEG cycles: 4 (1), MEG amplitude: 35 (15 to 35) mT m^{-1}, repetition time: $TR = 3.0$ (0.5) s, echo-time: $TE = 149$ (64) ms, FoV = 192 to 202 (300) mm,

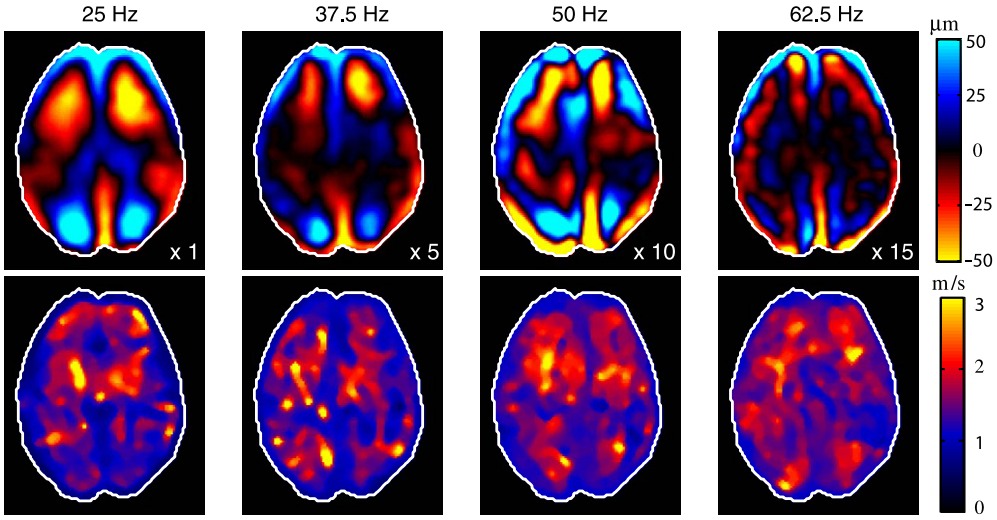

Figure 3. Top row: real part of complex wave images after Fourier decomposition of the acquired superposition of brain vibrations in volunteer 1. The factors given in the lower right corner of the wave images were used for scaling the individual color axes to similar contrasts. Bottom row: the corresponding shear wave-speed contrast images calculated using equation (4).

matrix size 128 × 128 (64 × 128), slice thickness = 6 (10) mm, total measurement time = 4 min (40 s, divided into two breath-holds).

Wave generation

Shear waves were introduced into brain and liver by a custom-built vibration generator as recently described in Klatt *et al* (2006). Four frequencies of 25, 37.5, 50 and 62.5 Hz were superposed with linearly increasing amplitude to minimize transient effects and increase patient comfort (figure 2). The broad-band spectral sensitivity of the MEG resulted in motion-encoding factors of 5 (8), 8 (10), 14 (9) and 29 (7) × 10^{-2} rad μm^{-1} at the four increasing driving frequencies, assuming a 35 mT m^{-1} gradient strength and the corresponding brain (liver) MEG adjustments as given above. In the brain study all four frequencies were superposed with the same amplitude, whereas in the liver studies the amplitude ratios were 1, 2, 4 and 8 relative to the 25 Hz vibration.

Data processing

Phase-difference wave images were temporally Fourier transformed and complex wave images $U(x, y, \omega)$ were taken at 25, 37.5, 50 and 62.5 Hz. Then, a spatial 2D Butterworth filter was applied to suppress compression wave components and noise using isotropic lower thresholds of 6.7 (3.2) m^{-1}, 12.3 (5.7) m^{-1}, 16.9 (8.6) m^{-1} and 20.8 (13.2) m^{-1} and upper thresholds of 82.6 (73.7) m^{-1}, 84.4 (80.7) m^{-1}, 82.6 (82.9) m^{-1} and 104.4 (104.4) m^{-1} in brain (liver) wave images at the four increasing driving frequencies, respectively. $G(\omega)$ was then calculated according to equation (2) assuming a density of 1050 kg m^{-3} and either averaging the spatially resolved modulus over the entire brain or within a wave-energy-dependent region of interest of the liver, as previously described (Klatt *et al* 2006). $G(\omega)$ was used in equation (4) to derive the phase velocities $c(\omega)$ and the damping coefficients $\gamma(\omega)$.

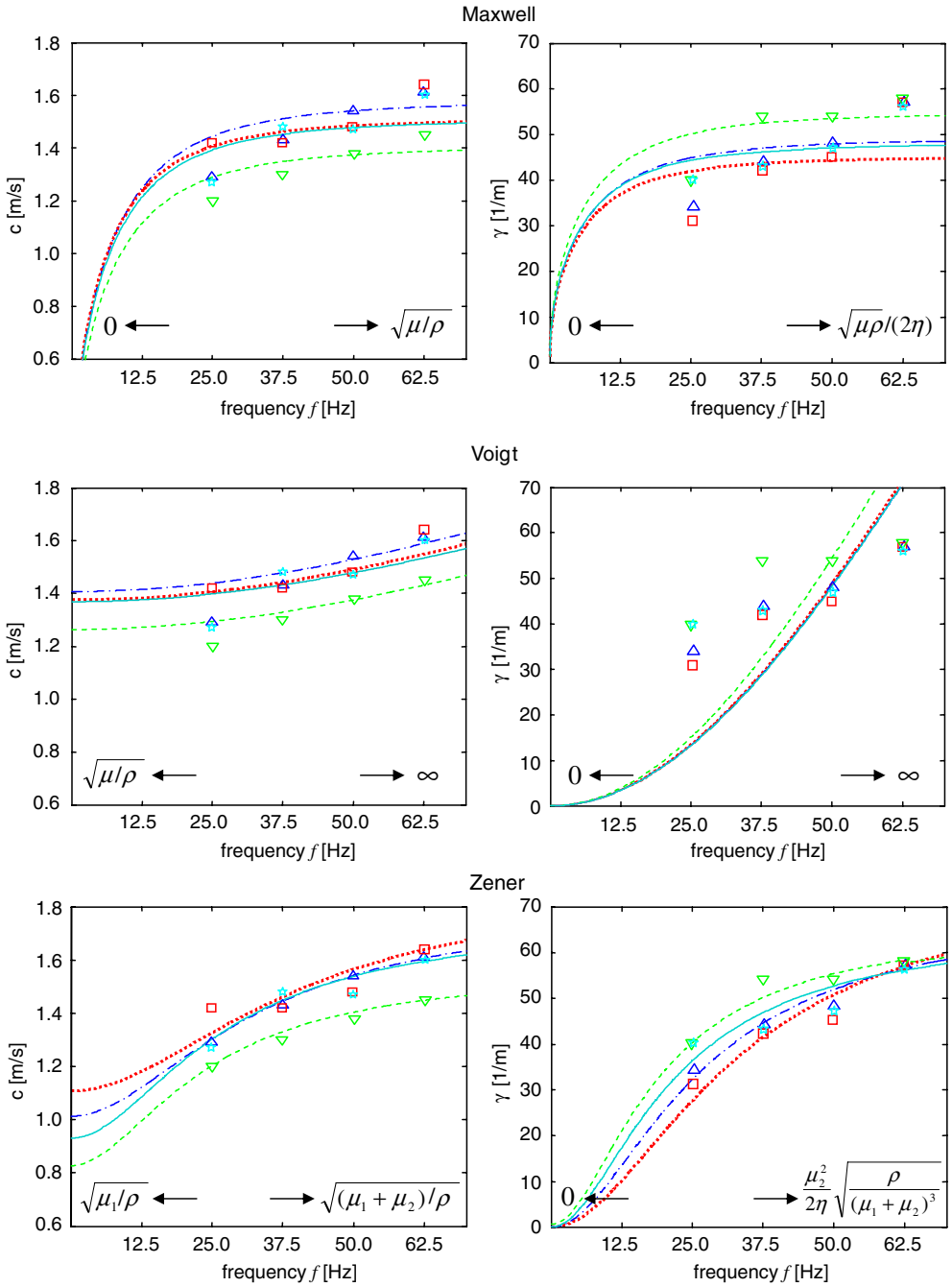

Figure 4. Experimental (symbols) and simulated (line graphs) wave-speed and wave-damping dispersion relations found for the brain of volunteer 1 by four follow-up experiments. The colors/symbols/line-styles: blue/triangle-up/dash-dot, red/square/dot, green/triangle-down/dash and cyan/asterisk/solid correspond to the experiments 1 to 4 of table 1, respectively. The expressions or numbers next to the arrows give the low frequency limit (←) and the high frequency limit (→) of the wave speed and the wave damping.

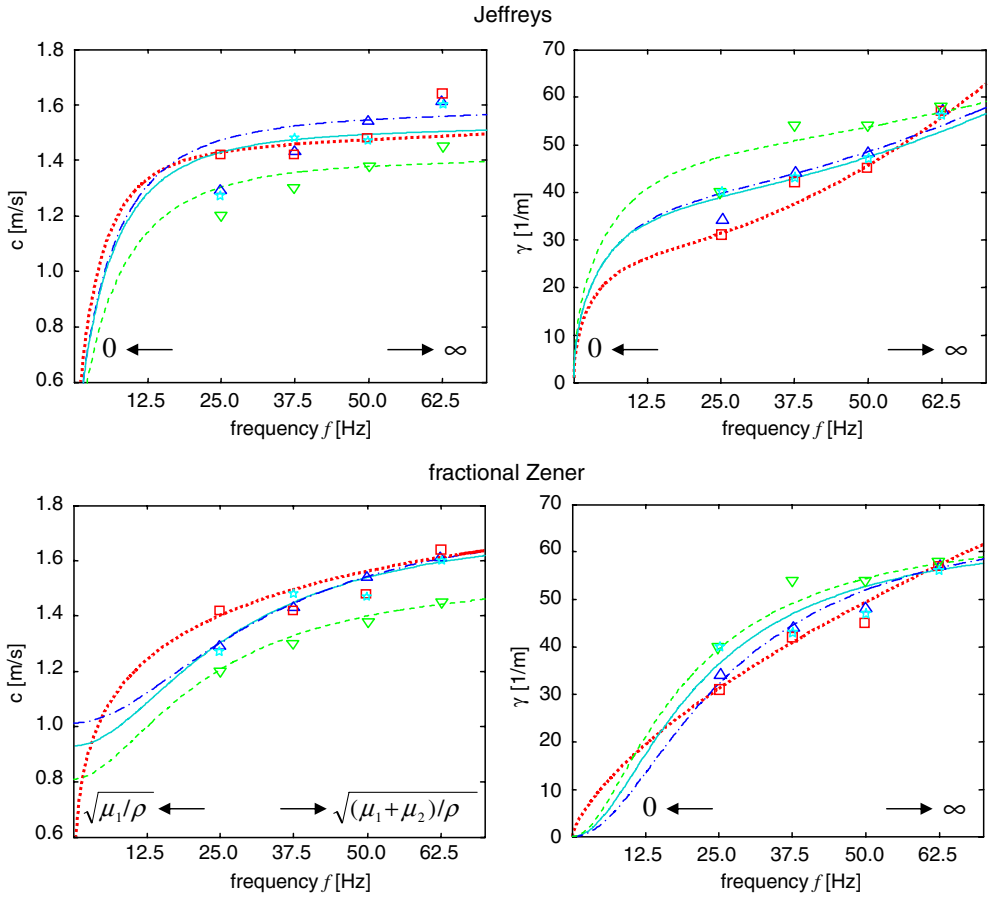

Figure 4. (Continued.)

Determination of viscoelastic parameters

Model-dependent complex moduli $G_M(\omega)$ were calculated according to equation (5), using variable viscoelastic parameters. The variation between $G_M(\omega)$ and $G(\omega)$ given by χ (equation (6)) was stored in memory for the entire viscoelastic parameter space. The parameters resulting in the global minimum of χ were taken as best-fit variables of the rheological model used for one single experiment. The procedure was repeated four times for each volunteer, corresponding to the number of follow-up studies. The individual mean viscoelastic parameters (labeled by an asterisk *) and their standard deviations (SD) were calculated from these four independent studies. Then, the corresponding error χ^* was derived from the mean model modulus $G_M(\omega)^*$ and the mean experimental modulus $G(\omega)^*$ using equation (6). Furthermore, $G_M(\omega)^*$ and $G(\omega)^*$ were used to calculate the interindividual average (henceforth, labeled by two asterisks **) for assessing the significance of the viscoelastic properties of liver and brain. χ^{**} was derived by inserting $G_M(\omega)^{**}$ and $G(\omega)^{**}$ into equation (6). Please note that χ^* and χ^{**} are different from simply averaging χ or χ^*, respectively.

Table 1. Volunteer 1, brain experiments: viscoelastic parameters and error of the fit χ according to the models given in equation (5) and figure 1 and derived from four independent experiments (exp. 1–4).

Model		Exp. 1	Exp. 2	Exp. 3	Exp. 4	Mean*
Maxwell	η (Pa s)	16.9	17.6	13.5	16.5	16.1 (1.8)
	μ (kPa)	2.64	2.42	2.10	2.41	2.39 (0.22)
	χ (kPa)	0.24	0.25	0.16	0.20	0.19
Voigt	η (Pas)	3.3	3.1	2.7	3.0	3.0 (0.2)
	μ (kPa)	2.08	1.99	1.68	1.97	1.93 (0.17)
	χ (kPa)	0.38	0.36	0.34	0.40	0.36
Zener	η (Pa s)	6.3	5.6	6.5	7.2	6.4 (0.7)
	μ_1 (kPa)	1.08	1.29	0.72	0.91	1.00 (0.24)
	μ_2 (kPa)	2.27	2.42	1.82	2.26	2.19 (0.26)
	χ (kPa)	0.05	0.17	0.05	0.12	0.08
Jeffreys	η_1 (Pa s)	20.6	27.9	14.8	20.4	20.9 (5.4)
	η_2 (Pa s)	0.8	1.3	0.3	0.7	0.8 (0.4)
	μ (kPa)	2.64	2.32	2.11	2.45	2.38 (0.22)
	χ (kPa)	0.23	0.16	0.16	0.19	0.19
Fractional Zener	η (Pa s)	6.3	6.9	6.7	7.2	6.8 (0.4)
	μ_1 (kPa)	1.08	0.00	0.69	0.91	0.67 (0.47)
	μ_2 (kPa)	2.27	5.94	1.85	2.26	3.08 (1.91)
	α	1.00	0.49	0.98	1.00	0.87 (0.25)
	χ (kPa)	0.05	0.15	0.05	0.12	0.21

* Here, the viscoelastic constants of experiments 1 to 4 were averaged (mean with SD in brackets) except for χ^* which was gained by equation (6) and using the mean viscoelastic parameters (see the methods section).

Results

Figure 3 shows a multifrequent-MRE data sample of the brain of volunteer 1 decomposed into the four frequencies used for the vibration signal. The factors in the lower right corner of the wave images indicate the decrease of wave amplitude with increasing frequency. Nevertheless, the signal-to-noise ratio was similar for all four frequencies due to the higher motion sensitivity of the MEG with increasing vibration frequency (see the methods section). The respective shear wave-speed contrast images are shown below the wave images. It is already perspicuous from visual inspection that the wave speed increases with higher excitation frequencies.

Figure 4 demonstrates the fit of c- and γ-dispersion data measured in the brain of volunteer 1 by the rheological models of equation (5). Similar dispersion curves were obtained by repeating the wave data acquisition for each frequency component under monochromatic excitation (data not shown). Viscoelastic parameters which correspond to the model curves as well as the variation between fit and data are given in table 1. Considering single experiments, the quality of the fit χ is improved with an increasing number of independent fit parameters from two to three. However, no further improvement of the fit is achieved by substituting the three-parameter Zener model with the four-parameter fractional one. This finding is supported by χ^*, which is even larger in the four-parameter model than in the Zener model. Among the two-parameter models, the Maxwell model is favored over the Voigt model ($\chi^* = 0.19$ versus 0.36 kPa), while the Zener model is preferred to the Jeffreys model ($\chi^* = 0.08$ versus 0.19 kPa) when using three parameters. The fractional Zener model well reproduces single experiments with equal or smaller χ values than those achieved by the Zener model. However,

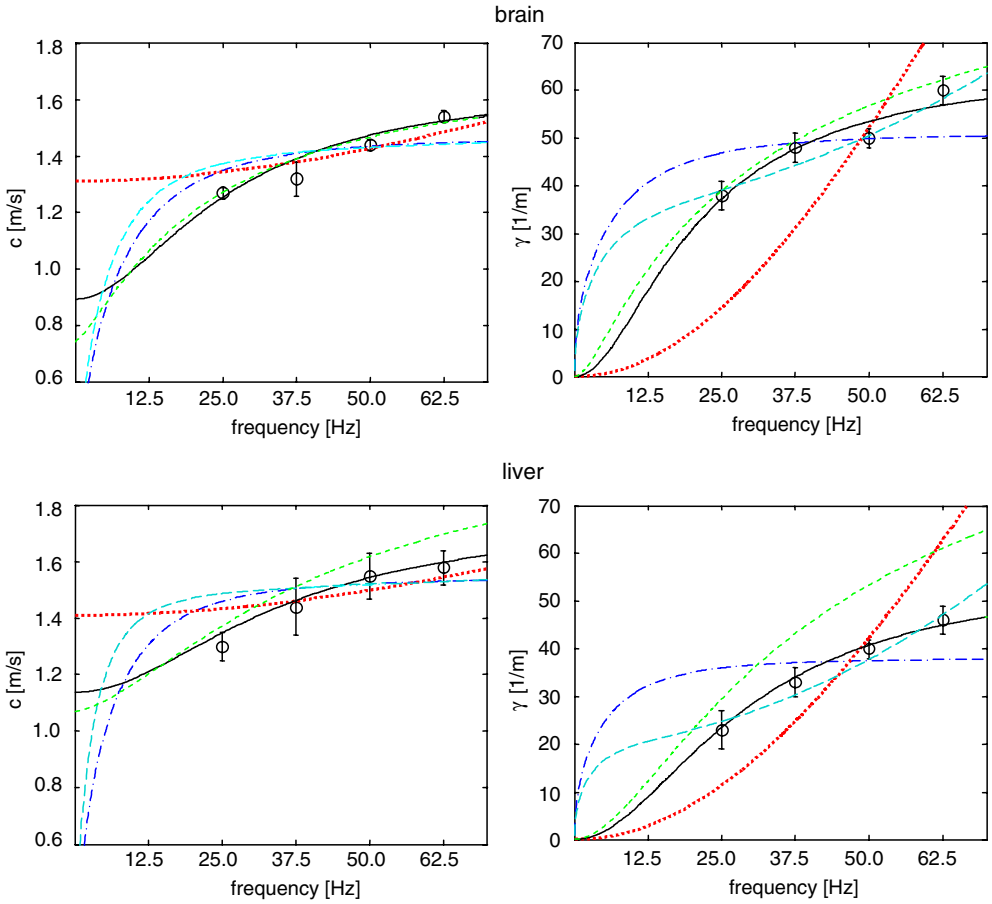

Figure 5. Dispersion relation found for the wave speed (left column) and the wave damping (right column) in brain and liver according to the Maxwell (dash-dotted, blue line) Voigt (dotted, red line), Zener (solid, black line), Jeffreys (long-dashed, cyan line) and fractional Zener models (short-dashed, green line). The experimental interindividual mean data are displayed as circles.

it was empirically found by χ^* that the variation of the experimental data causes instability of the four-parameter fit. As is shown in table 1, standard deviations of the elastic moduli are larger according to the fractional Zener model than to the Zener model. Also, the range of α-values given in table 1 from 0.49 to 1.0 is ambiguous. While experiments 1, 3 and 4 indicate the insignificance of α, experiment 2 was slightly better matched by a low α-value combined with a tremendous increase of the difference $\mu_2 - \mu_1$. The inexpedience of the four-element model is also seen in figure 5, showing the interindividual mean of all data together with the mean of the corresponding fit curves. In both brain and liver, the best agreement between fit and experiment was achieved again with the Zener model. Among the two-parameter models, the Maxwell model reproduces the dispersion of our data better than the Voigt model. The error χ^* of each individual fit with corresponding viscoelastic parameters is listed in tables 2 and 3 for brain and liver, respectively.

Here, the Zener model is further considered for a comparison of viscoelastic properties of brain and liver. Combining all experimental data yielded $\eta = 6.7 \pm 1.3$ Pa s, $\mu_1 = 0.84 \pm 0.22$ kPa and $\mu_2 = 2.03 \pm 0.19$ kPa for the brain, while $\eta = 5.5 \pm 1.6$ Pa s, $\mu_1 = 1.36 \pm$

Table 2. Results of the brain experiments: mean viscoelastic parameters and χ^* of the brain of five volunteers (vol. 1–5) according to five rheological models (SD in brackets). The asterisk indicates that the given quantities are averaged over four independent experiments. The interindividual mean and SD (**) of the viscoelastic parameters are shown in the last column, whereas χ^{**} is the result of equation (6) using the interindividual mean modulus values (see the methods section).

Model		Vol. 1	Vol. 2	Vol. 3	Vol. 4	Vol. 5	Mean (**)
Maxwell	η^* (Pa s)	16.1	14.6	14.1	14.7	16.1	15.1
		(1.8)	(0.9)	(0.9)	(0.2)	(1.0)	(0.9)
	μ^* (kPa)	2.39	2.20	2.23	2.27	2.30	2.28
		(0.22)	(0.14)	(0.09)	(0.08)	(0.08)	(0.07)
	χ^* (kPa)	0.19	0.22	0.19	0.29	0.20	0.21
Voigt	η^* (Pa s)	3.0	2.9	3.0	2.9	2.8	2.9
		(0.2)	(0.2)	(0.1)	(0.2)	(0.2)	(0.1)
	μ^* (kPa)	1.93	1.75	1.72	1.78	1.86	1.81
		(0.17)	(0.11)	(0.09)	(0.05)	(0.08)	(0.08)
	χ^* (kPa)	0.36	0.38	0.34	0.35	0.33	0.35
Zener	η^* (Pa s)	6.4	7.5	7.6	5.2	6.7	6.7
		(0.7)	(0.3)	(2.0)	(0.1)	(1.3)	(1.0)
	μ_1^* (kPa)	1.00	0.67	0.65	1.00	0.87	0.84
		(0.24)	(0.10)	(0.24)	(0.08)	(0.13)	(0.17)
	μ_2^* (kPa)	2.19	1.85	2.03	2.10	1.96	2.03
		(0.26)	(0.06)	(0.13)	(0.20)	(0.10)	(0.13)
	χ^* (kPa)	0.08	0.13	0.11	0.14	0.09	0.10
Jeffreys	η_1^* (Pa s)	20.9	16.7	18.5	23.9	20.7	20.1
		(5.4)	(2.2)	(4.2)	(2.1)	(1.4)	(2.7)
	η_2^* (Pa s)	0.8	0.4	0.9	1.5	0.9	0.9
		(0.4)	(0.3)	(0.6)	(0.2)	(0.1)	(0.4)
	μ^* (kPa)	2.38	2.19	2.14	2.16	2.26	2.23
		(0.22)	(0.13)	(0.20)	(0.11)	(0.07)	(0.10)
	χ^* (kPa)	0.19	0.22	0.18	0.27	0.18	0.20
Fractional Zener	η^* (Pa s)	6.8	8.4	9.7	5.7	8.7	7.8
		(0.4)	(0.8)	(2.9)	(0.4)	(2.1)	(1.6)
	μ_1^* (kPa)	0.67	0.55	0.36	0.72	0.58	0.58
		(0.47)	(0.14)	(0.28)	(0.10)	(0.21)	(0.14)
	μ_2^* (kPa)	3.08	2.05	2.57	3.08	2.52	2.66
		(1.91)	(0.03)	(0.40)	(0.53)	(0.38)	(0.44)
	α^*	0.87	0.93	0.85	0.78	0.85	0.85
		(0.25)	(0.03)	(0.05)	(0.08)	(0.10)	(0.06)
	χ^* (kPa)	0.21	0.12	0.10	0.14	0.08	0.12

0.31 kPa and $\mu_2 = 1.86 \pm 0.34$ kPa was found for the liver (the tolerances correspond to confidence intervals with $P < 0.05$). A student t-test revealed significant variations in η, μ_1 and $\mu_1 + \mu_2$ among both organs ($P < 0.05$) (figure 6).

Discussion

It was demonstrated that the rheological behavior of soft tissue can be noninvasively characterized by multifrequent MRE. Simultaneous excitation of shear vibrations using four frequencies combined with a broad-band motion-encoding gradient enables the measurement of the dynamics of the tissue's strain response in a quarter of the conventionally required

Table 3. Results of the liver experiments: mean viscoelastic parameters (SD in brackets) and χ^* of the liver of five volunteers (vol. 1–5). * indicates that the given quantities are averaged over the simulations of four independent experiments. The interindividual mean and SD of the viscoelastic parameters (**) are shown in the last column (except for χ^{**} which is the result of equation (6) using $G(\omega)^{**}$ and $G_M(\omega)^{**}$ as described in the methods section).

Model		Vol. 1	Vol. 2	Vol. 3	Vol. 4	Vol. 5	Mean (**)
Maxwell	η^* (Pa s)	23.6	22.5	21.5	20.7	18.0	21.3
		(2.2)	(3.6)	(2.0)	(2.2)	(2.5)	(2.1)
	μ^* (kPa)	2.81	2.57	2.40	2.60	2.21	2.52
		(0.44)	(0.28)	(0.11)	(0.20)	(0.12)	(0.23)
	χ^* (kPa)	0.33	0.39	0.21	0.26	0.28	0.28
Voigt	η^* (Pa s)	3.0 (0.6)	2.9 (0.5)	2.6 (0.3)	2.9 (0.1)	2.4 (0.3)	2.8 (0.3)
	μ^* (kPa)	2.41	2.06	2.03	2.13	1.80	2.09
		(0.36)	(0.23)	(0.06)	(0.22)	(0.15)	(0.22)
	χ^* (kPa)	0.35	0.41	0.32	0.29	0.27	0.31
Zener	η^* (Pa s)	5.0 (0.6)	5.3 (0.6)	7.3 (2.5)	5.8 (1.5)	4.1 (0.3)	5.5 (1.2)
	$\mu_1{}^*$ (kPa)	1.75	1.39	1.05	1.36	1.23	1.36
		(0.39)	(0.18)	(0.25)	(0.06)	(0.09)	(0.26)
	$\mu_2{}^*$ (kPa)	2.17	1.90	1.73	1.90	1.62	1.86
		(0.58)	(0.32)	(0.14)	(0.12)	(0.14)	(0.21)
	χ^* (kPa)	0.16	0.19	0.06	0.11	0.07	0.08
Jeffreys	$\eta_1{}^*$ (Pa s)	58.0	37.1	28.9	41.5	42.6	41.6
		(32.5)	(11.4)	(7.8)	(9.3)	(2.2)	(10.6)
	$\eta_2{}^*$ (Pa s)	1.7 (0.7)	1.2 (0.6)	0.7 (0.4)	1.5 (0.4)	1.6 (0.3)	1.4 (0.4)
	μ^* (kPa)	2.69	2.59	2.37	2.43	1.96	2.41
		(0.32)	(0.32)	(0.08)	(0.26)	(0.21)	(0.28)
	χ^* (kPa)	0.31	0.37	0.19	0.19	0.24	0.25
Fractopnal Zener	η^* (Pa s)	5.0 (0.7)	5.4 (0.6)	12.0 (9.6)	4.4 (3.1)	4.2 (0.4)	6.2 (3.3)
	$\mu_1{}^*$ (kPa)	1.74	1.36	0.79	0.92	1.21	1.20
		(0.36)	(0.18)	(0.59)	(0.63)	(0.05)	(0.38)
	$\mu_2{}^*$ (kPa)	2.30	1.93	2.09	8.62	1.69	3.33
		(0.76)	(0.30)	(0.60)	(10.67)	(0.17)	(2.97)
	α^*	0.98	0.98	0.92	0.70	0.98	0.91
		(0.03)	(0.04)	(0.13)	(0.35)	(0.04)	(0.12)
	χ^* (kPa)	0.16	0.19	0.17	0.61	0.07	0.38

examination time in MRE. Apart from time considerations, additional information about the dynamics of the stress–strain relation enables fit-based data evaluation which mitigates experimental scattering of the wave-speed and wave-damping data. Among the tested rheological models, the Zener model well reproduces the dispersion of data seen in our experiments. This three-parameter model even compensates for the inherent experimental tolerances observed in follow-up studies. Therefore, adding an additional rheological parameter as given by α in the fractional Zener model will increase the variation of the results even though the adaptation of the fit to single experiments is improved.

A body obeying the Zener model displays convergent limits at static deformation ($G_M(\omega \to 0) = \mu_1$) and at high frequencies $G_M(\omega \to \infty) = \mu_1 + \mu_2$. These limits were found in figure 6 to be significantly lower in brain than in liver. Together with a

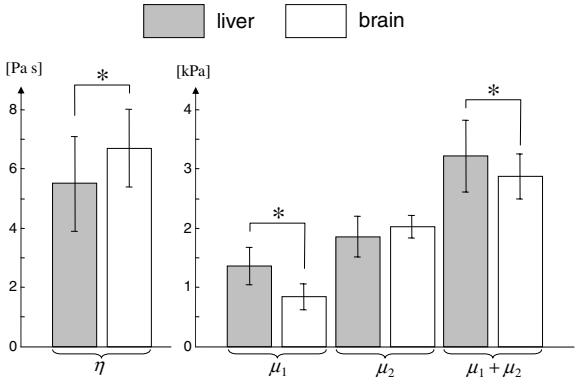

Figure 6. A comparison of brain and liver viscoelasticity according to the Zener model (*$P <$ 0.05).

significant higher viscosity, the global rheological behavior of brain tends to be softer and more dissipative than liver.

Our data suggest convergence in the high-frequency response of both organs, which is, however, not seen in most *ex vivo* tests (Valtorta and Mazza 2006, Liu and Bilston 2000, Nicolle *et al* 2005, Kiss *et al* 2004). Fabry *et al* (2003) have investigated the mechanical behavior of single cells showing that the complex modulus dynamics follows a power law determined by the so-called structural damping of the cytoskeleton. Robert *et al* (2006) similarly observed a power law in the complex modulus between 40 and 100 Hz driving frequency by MRE on liver specimen, suggesting the validity of scaling of the cellular viscoelasticity on a macroscopic level. In contrast, Kruse *et al* (2000) found good compliance of liver MRE data to the Voigt model in a dynamic range between 75 and 300 Hz, indicating a constant storage modulus. The dynamic function found in this study is between both MRE observations made on liver specimens.

In recent years, only a few MRE studies on human brain have been published that report a great variety of shear modulus data, ranging from 2.5 to 15.2 kPa for white matter and from 2.8 to 12.9 kPa for gray matter (McCracken *et al* 2005, Green *et al* 2005, Uffmann *et al* 2004). This variation may be attributed to the use of different excitation frequencies and different wave analysis methods. A 3D wave inversion was used in Green *et al* (2005) yielding a mean shear modulus of 2.5 kPa at 65 Hz, while Hamhaber *et al* (2007) found 3.5 kPa at 83 Hz using a 3D wave front tracking technique. A recently published 2D brain MRE study revealed mean shear moduli of 1.17 kPa and 1.56 kPa at 25 and 50 Hz, respectively (Sack *et al* 2007). The static modulus $\mu_1 = 0.84 \pm 0.22$ kPa corresponds well to this shear modulus dispersion curve, whereas the high frequency limit $\mu_1 + \mu_2 = 2.87 \pm 0.38$ kPa is below the results of other MRE work.

Further conclusions about rheological constants in living human organs will require an extension of the dynamic range. A superposition of additional multiples of the first harmonic driving frequency is restricted by both the encoding efficiency of the MEG over an extended spectral range and the increased damping of higher harmonic vibrations. For instance, we were not able to detect the 75 Hz vibration component by the current protocol. However, the emphasis in this study was on evaluating dispersed wave-speed and wave-damping data to increase the inherent accuracy of *in vivo* MRE. As such, multifrequent MRE combined with data evaluation based on the three-parameter Zener model provides a convenient means to shed light on tissue rheology within the clinically applicable examination time.

In summary, synchronous excitation and detection of multiple vibration frequencies enable us to increase the dynamic range of MRE wave-speed and wave-damping data without any additional scan time. The higher number of independent experimental data can be used to fit a rheological model which increases the specificity of MRE to the inherent viscoelastic behavior of biological soft tissue. In our current setup, four driving frequencies between 25 and 62.5 Hz allowed the rheological characterization of *in vivo* human brain and liver by the three-parameter Zener model.

References

Bayly P V, Black E E, Pedersen R C, Leister E P and Genin G M 2006 *In vivo* imaging of rapid deformation and strain in an animal model of traumatic brain injury *J. Biomech.* **39** 1086–95

Bensamoun S F, Ringleb S I, Littrell L, Chen Q, Brennan M, Ehman R L and An K N 2006 Determination of thigh muscle stiffness using magnetic resonance elastography *J. Magn. Reson. Imaging* **23** 242–7

Bercoff J, Chaffai S, Tanter M, Sandrin L, Catheline S, Fink M, Gennisson J L and Meunier M 2003 *In vivo* breast tumor detection using transient elastography *Ultrasound Med. Biol.* **29** 1387–96

Corpechot C *et al* 2006 Assessment of biliary fibrosis by transient elastography in patients with PBC and PSC *Hepatology* **43** 1118–24

Fabry B, Maksym G N, Butler J P, Glogauer M, Navajas D, Taback N A, Millet E J and Fredberg J J 2003 Time scale and other invariants of integrative mechanical behavior in living cells *Phys. Rev.* E **68** 041914

Fung Y 1993 *Biomechanics: Mechanical Properties of Living Tissue* (New York: Springer-Verlag)

Gennisson J L, Cornu C, Catheline S, Fink M and Portero P 2005 Human muscle hardness assessment during incremental isometric contraction using transient elastography *J. Biomech.* **38** 1543–50

Green M A, Sinkus R, Cheng S and Bilston L E 2005 3D MR-elastography of the brain at 3 Tesla *Proc. 13th Annual Meeting ISMRM (Miami)* p 2176

Hamhaber U, Sack I, Papazoglou S, Rump J, Klatt D and Braun J 2007 Three-dimensional analysis of shear wave propagation observed by *in vivo* magnetic resonance elastography of the brain *Acta Biomater.* **3** 127–37

Huwart L, Peeters F, Sinkus R, Annet L, Salameh N, ter Beek L C, Horsmans Y and Van Beers B E 2006 Liver fibrosis: non-invasive assessment with MR elastography *NMR Biomed.* **19** 173–9

Joseph D D 1990 *Fluid Dynamics of Viscoelastic Liquids* (Berlin: Springer) p 755

Kiss M Z, Varghese T and Hall T J 2004 Viscoelastic characterization of *in vitro* canine tissue *Phys. Med. Biol.* **49** 4207–18

Klatt D, Asbach P, Rump J, Papazoglou S, Somasundaram R, Modrow J, Braun J and Sack I 2006 *In vivo* determination of hepatic stiffness using steady-state free precession magnetic resonance elastography *Invest. Radiol.* **41** 841–8

Kruse S A, Smith J A, Lawrence A J, Dresner M A, Manduca A, Greenleaf J F and Ehman R L 2000 Tissue characterization using magnetic resonance elastography: preliminary results *Phys. Med. Biol.* **45** 1579–90

Kuroiwa T, Yamada I, Katsumata N, Endo S and Ohno K 2006 *Ex vivo* measurement of brain tissue viscoelasticity in postischemic brain edema *Acta Neurochir. Suppl.* **96** 254–7

Liu Z and Bilston L 2000 On the viscoelastic character of liver tissue: experiments and modelling of the linear behaviour *Biorheology* **37** 191–201

McCracken P J, Manduca A, Felmlee J and Ehman R L 2005 Mechanical transient-based magnetic resonance elastography *Magn. Reson. Med.* **53** 628–39

Muthupillai R, Lomas D J, Rossman P J, Greenleaf J F, Manduca A and Ehman R L 1995 Magnetic resonance elastography by direct visualization of propagating acoustic strain waves *Science* **269** 1854–7

Nicolle S, Lounis M, Willinger R and Palierne J F 2005 Shear linear behavior of brain tissue over a large frequency range *Biorheology* **42** 209–23

Papazoglou S, Rump J, Braun J and Sack I 2006 Shear-wave group-velocity inversion in MR elastography of human skeletal muscle *Magn. Reson. Med.* **56** 489–97

Parker K J, Fu D, Graceswki S M, Yeung F and Levinson S F 1998 Vibration sonoelastography and the detectability of lesions *Ultrasound Med. Biol.* **24** 1437–47

Robert B, Sinkus R, Bercoff J, Tanter M and Fink M 2006 A novel fractal model to explain the rheology of liver tissue using mr-elastography *Proc. 14th Annual Meeting of ISMRM (Seattle)* p 2560

Rouviere O, Yin M, Dresner M A, Rossman P J, Burgart L J, Fidler J L and Ehman R L 2006 MR elastography of the liver: preliminary results *Radiology* **240** 440–8

Rump J, Klatt D, Braun J, Warmuth C and Sack I 2007 Fractional encoding of harmonic motions in MR elastography *Magn. Reson. Med.* **57** 388–95

Sack I, Beierbach B, Hamhaber U, Klatt D and Braun J 2007 Rapid noninvasive measurement of brain viscoelasticity using magnetic resonance elastography *NMR Biomed.* at press doi:10.1002/nbm.1189

Schiessel H, Metzler R, Blumen A and Nonnenmacher T F 1995 Generalized viscoelastic models: their fractional equations with solutions *J. Phys. A: Math. Gen.* **28** 6567–84

Scholz M *et al* 2005 Vibrography during tumor neurosurgery *J. Ultrasound Med.* **24** 985–92

Sinkus R, Tanter M, Xydeas T, Catheline S, Bercoff J and Fink M 2005 Viscoelastic shear properties of *in vivo* breast lesions measured by MR elastography *Magn. Reson. Imaging* **23** 159–65

Taylor Z and Miller K 2004 Reassessment of brain elasticity for analysis of biomechanisms of hydrocephalus *J. Biomech.* **37** 1263–9

Uffmann K, Maderwald S, Ajaj W, Galban C G, Mateiescu S, Quick H H and Ladd M E 2004 *In vivo* elasticity measurements of extremity skeletal muscle with MR elastography *NMR Biomed.* **17** 181–90

Uffmann K, Maderwald S, de Greiff A and Ladd M 2004 Determination of gray and white matter elasticity with MR elastography *Proc. 12th Annual Meeting of ISMRM (Kyoto)* p 1768

Valtorta D and Mazza E 2006 Measurement of rheological properties of soft biological tissue with a novel torsional resonator device *Rheol. Acta* **45** 677–92

Van Houten E E, Doyley M M, Kennedy F E, Weaver J B and Paulsen K D 2003 Initial *in vivo* experience with steady-state subzone-based MR elastography of the human breast *J. Magn. Reson. Imaging* **17** 72–85

Ziol M *et al* 2005 Noninvasive assessment of liver fibrosis by measurement of stiffness in patients with chronic hepatitis C *Hepatology* **41** 48–54